Hexa-*peri*-hexabenzocoronene on Ag(111): Monolayer/Multilayer Transition of Molecular Orientation and Electronic Structure

H. Glowatzki,[†] G. N. Gavrila,[‡] S. Seifert,[‡] R. L. Johnson,[§] J. Räder,[||] K. Müllen,[||] D. R. T. Zahn,[‡] J. P. Rabe,[†] and N. Koch*,[†]

Humboldt-Universität zu Berlin, Institut f. Physik, Newtonstr. 15, D-12489 Berlin, Germany, Technische Universität Chemnitz, Institut f. Physik, Reichenhainer Str. 70, D-09126 Chemnitz, Germany, Universität Hamburg, Institut f. Experimentalphysik, D-22761 Hamburg, Germany, and Max Planck Institut für Polymerforschung, D-55021 Mainz, Germany

Received: September 17, 2007; In Final Form: November 4, 2007

The molecular orientation and electronic structure of hexa-*peri*-hexabenzocoronene (HBC) deposited on Ag(111) was investigated in the mono- and multilayer regime by near edge X-ray absorption fine structure spectroscopy (NEXAFS), scanning tunneling and scanning force microscopy (STM and SFM), and ultraviolet photoelectron spectroscopy (UPS). We found that the molecular orientation changed as a function of coverage, exhibiting a transition from flat lying HBC in the monolayer to molecules being 43° inclined relative to the substrate plane in the multilayer. This structural transition was accompanied by a rigid shift of molecular energy levels by 0.3 eV toward higher binding energy between mono- and multilayer. In addition, broadening of the highest molecular levels by ca. 0.35 eV was observed in the multilayer, suggesting the formation of extended intermolecular energy bands.

Introduction

Electronic devices based on conjugated organic molecules are presently receiving considerable attention. Organic light emitting diodes, solar cells, thin film transistors, and memory elements have been realized, which demonstrates the huge potential of realizing a new technology platform.[1] Interfaces between metal electrodes and organic materials are ubiquitous in such devices. Consequently, the understanding of the organic/metal interface properties is a key factor to optimize organic electronic device function. In particular, the interplay between structural and electronic properties is of huge interest. One prototypical molecule in the context of organic electronics is hexa-*peri*-hexabenzocoronene (HBC; Figure 1). Because of the disc-like structure and high-symmetry, HBC forms highly ordered layers on many substrate materials, including, e.g., highly oriented pyrolytic graphite (HOPG),[2] Cu(111),[3] and Au(111).[4] In the bulk crystal, HBC packs in columns with the molecular discs in one column being tilted in one direction with respect to the column normal, whereas in neighboring columns, the tilt direction is different.[5−7] Because of the parallel stacking of the molecular π systems, large charge carrier mobilities along the columns are expected.[8] An alkyl substituted derivate of HBC, hexakis-dodecyl-hexabenzocoronene (C_{12}HBC), has been shown to exhibit a high one-dimensional carrier mobility of 0.5 cm^2/Vs.[9] A number of other derivatives of HBC have been investigated,[10] indicating that HBC is of interest also in the field of molecular electronics, e.g., for realizing molecular nanowires,[11,12] molecular diodes,[13,14] or a single molecule transistor.[15]

In order to obtain a better understanding of the growth and electronic structure of this prototypical molecule on a metal electrode, we investigated HBC on Ag(111) from the monolayer to the multilayer regime. The orientation of the molecules was determined using near edge X-ray absorption fine structure spectroscopy (NEXAFS), scanning tunneling and scanning force microscopy (STM and SFM), and information on electronic properties was obtained from ultraviolet photoemission spectroscopy (UPS).

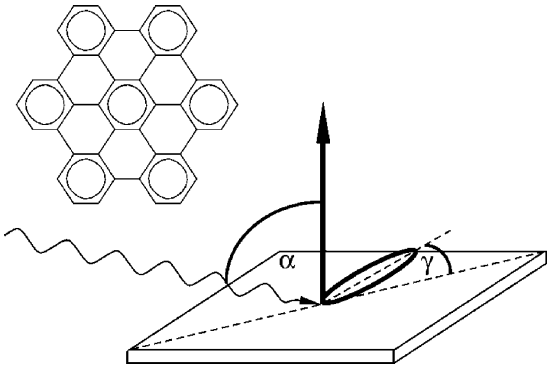

Figure 1. Chemical structure of HBC and the geometry of the NEXAFS experiment showing the angle of photon incidence α and the angle of molecular plane orientation γ with respect to the sample surface.

Experimental Section

NEXAFS measurements were done at the Russian−German beamline at the synchrotron light source BESSY (Berlin, Germany), and UPS at the Flipper II endstation at Hasylab (Hamburg, Germany). In both experimental setups, sample preparation proceeded in a preparation chamber (base pressure 2×10^{-9} mbar) interconnected to the respective analysis chambers. Cleaning of Ag(111) was accomplished by repeated cycles of heating and sputtering. The cleanness of the surface was verified by photoelectron spectroscopy. As observed by

* To whom correspondence should be addressed.
[†] Humboldt-Universität zu Berlin.
[‡] Technische Universität Chemnitz.
[§] Universität Hamburg.
[||] Max Planck Institut für Polymerforschung.

10.1021/jp0774894 CCC: $40.75
Published on Web 01/15/2008

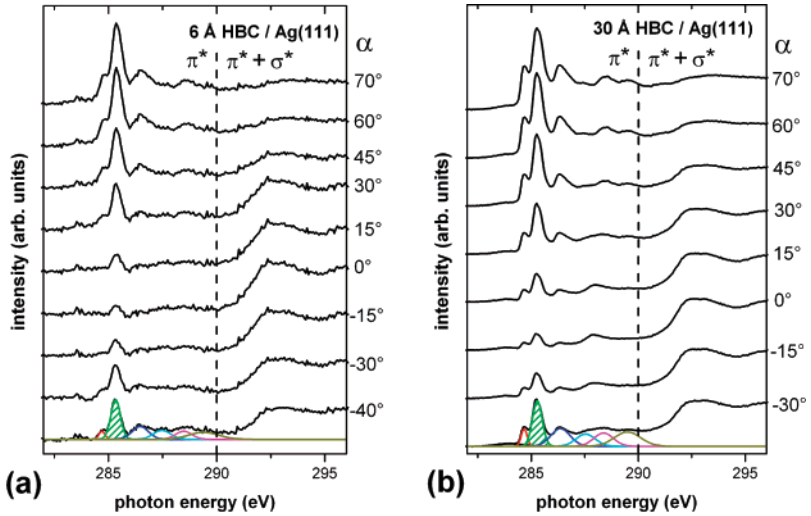

Figure 2. NEXAFS spectra of HBC on Ag(111) for different angles of photon incidence α for (a) 6 Å HBC coverage and (b) 30 Å coverage. The bottom spectra show the results of fitting the π^* region with six Gaussian peaks. The peak at 285.3 eV (shaded) was used for quantification of molecular orientation (see Figure 3).

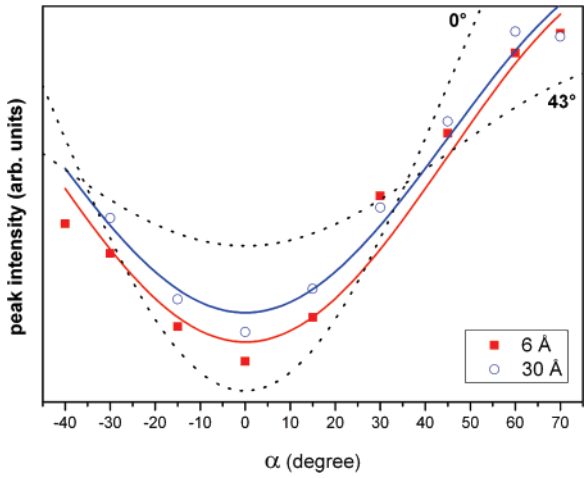

Figure 3. Peak intensity (obtained from the area of the NEXAFS feature at 285.3 eV in Figure 2) as function of the angle of photon incidence α. Filled red squares: 6 Å HBC coverage, open blue circles: 30 Å HBC coverage. The red (bottom) and blue (upper) solid lines represent the best fits to the data (see text for details). Dotted lines: calculated curves for $\gamma = 0°$ and 43°, according to eq 1.

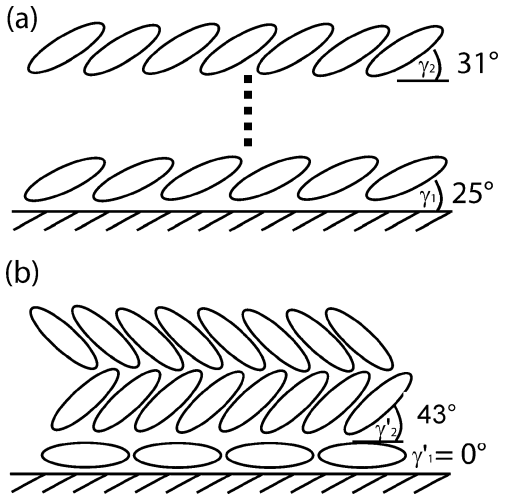

Figure 4. Proposed molecular orientation for mono- and multilayer HBC/Ag(111). (a) Model 1. (b) Model 2, as explained in the text.

STM, the crystal surface used in the experiments was atomically flat with a typical terrace width of 100 nm. HBC was evaporated from resistively heated pinhole sources. The mass thickness (assumed film thickness for a homogeneous molecular layer in the absence of island growth) of the deposited films was determined by a quartz microbalance. Separate atomic force microscopy measurements confirmed that the same mass was deposited on the microbalance and the substrate. After thin film deposition, samples were transferred to the respective analysis chambers without breaking ultrahigh vacuum (UHV) conditions.

NEXAFS spectra were obtained by sweeping the excitation energy between 280 and 320 eV and recording electrons having a selected kinetic energy of 6 eV using a Phoibos 150 hemispherical analyzer (SPECS GmbH). The pressure during measurements was 5×10^{-10} mbar. For angular dependent NEXAFS measurements, the angle of incidence on the sample α (see Figure 1) was varied stepwise from −40° to +70°, with 0° referring to normal incidence of the photon beam on the sample surface. All spectra were normalized (i) to the normal step edge spectrum of the clean Ag(111) crystal, to eliminate the system specific contribution to the carbon signal, and (ii) to the intensity at 320 eV photon energy, according to an established routine.[16] UPS spectra were obtained with a double-pass cylindrical mirror analyzer (resolution set to 150 meV) in an analysis chamber at a pressure of 2×10^{-10} mbar. The photon energy was set to 22 eV. STM and SFM measurements were done using an Omicron VT−STM attached to a custom UHV system at Humboldt University Berlin.

Results and Discussion

1. Molecular Orientation. In order to determine the molecular orientation of HBC on Ag(111), we used two different nominal coverages, i.e., 6 Å for the ca. monolayer regime and 30 Å for multilayer properties. For both samples, NEXAFS spectra from $\alpha = -40°$ to +70° were recorded (Figure 2). Several distinct absorption peaks are clearly visible near 285 eV below the C K-edge in both series of spectra and agree well with earlier published NEXAFS spectra of HBC.[2,17] With the help of theoretical calculations,[17] the peaks can be assigned to π^* resonances from five inequivalent carbon sites within a HBC molecule. As evident from the spectra, the intensity of the π^* peaks varies with α, and a clear minimum at $\alpha = 0°$ was found for both coverages. For the transition of an electron from the C K-shell into π^* states (as is the case here), the maximum

intensity is observed if the electric field vector of linearly polarized radiation is parallel to the long axis of the π^* orbital.[18] Since the π^* orbitals of HBC are oriented perpendicularly to the molecular plane, low absorption intensity at small α indicates a small angle γ between the molecular plane and the sample surface (see Figure 1). For spectral fitting, six Gaussian functions were used to reproduce the π^* region situated below 290 eV, as shown in the bottom spectra of Figure 2. For quantitative analysis, we chose the second peak at 285.3 eV (shaded in Figure 2) because it has the highest intensity and can also be reliably fitted for the 6 Å coverage spectra. The resulting dependence of this peak's area on α is shown in Figure 3 for the ca. monolayer (filled red squares) and the multilayer (open blue circles) samples. The relative peak areas were normalized to the one at 36°, for which the area is independent of the molecular orientation (cf. eq 1 below). The highest intensity and therefore strongest overlap between electric field vector and molecular π^* orbitals is found for large α, corresponding to small γ. From theoretical considerations for homogeneous layers, the angular dependence of the intensity I_{π^*} follows:[19,18]

$$I_{\pi^*} \sim P[\sin^2\gamma \sin^2(90° - \alpha) + 2\cos^2\gamma \cos^2(90° - \alpha)] + (1 - P)\sin^2\gamma \quad (1)$$

Here, $P = 0.98$ is the degree of photon beam polarization, which is characteristic of the beam source. Fits based on the experimental data are included in Figure 3, the bottom solid line (red) for the ca. monolayer and the upper solid line (blue) for the multilayer samples, respectively. For comparison, calculated dependencies according to eq 1 for $\gamma = 0°$ and 43° (this particular choice is justified further below) were also included as dotted lines. From this fitting procedure, the angle γ between molecular plane and sample plane was determined to $\gamma_1 = (25 \pm 4)°$ for 6 Å coverage and $\gamma_2 = (31 \pm 2)°$ for 30 Å coverage. In this model (model 1), the HBC molecules in the monolayer regime are already tilted with respect to the sample surface by γ_1, and the tilt angle increases slightly to γ_2 in thicker films (see Figure 4a). However, this simple model may be easily challenged, since all reports available at present indicate that conjugated molecules in a monolayer favor to align their π-electron systems parallel to a metal surface.[20−23] Furthermore, both angles, γ_1 and γ_2, do not occur in any known crystal structure of HBC,[5,6] which requires the presence of two yet unreported HBC polymorphs. Alternatively, the HBC films on Ag(111) could be amorphous with thickness-dependent average angles γ_1 and γ_2, which is rather unlikely for this type of discotic system. Therefore, we suggest an alternative model (model 2), which is built on known fundamental interfacial mechanisms and HBC properties already established in the literature, together with the fact that NEXAFS spectra contain information on more than the topmost molecular layer simultaneously. In this model, HBC molecules in the monolayer lie flat on the Ag(111) surface with $\gamma_1' = 0°$, in accordance with general expectations.[24,4] Molecules in the multilayer have a different orientation because of a reduced interaction strength with the metal surface, which is screened by the monolayer. Well defined and considerable changes in molecular orientation between mono- and multilayer on metal surfaces have been reported, e.g., for pentacene[25,26] and α,ω-dihexylsexithiophene.[21] For HBC, it could be expected that the multilayer aggregates in the known bulk crystal structure,[5] with the substrate surface [now comprising the HBC monolayer on Ag(111)] perpendicular to the HBC (010) net plane. In this scenario, the molecular plane in the bulk crystal forms an angle of $\gamma_2' = 43°$ with respect to the surface plane.[5] The angular dependence of π^* resonances found in NEXAFS

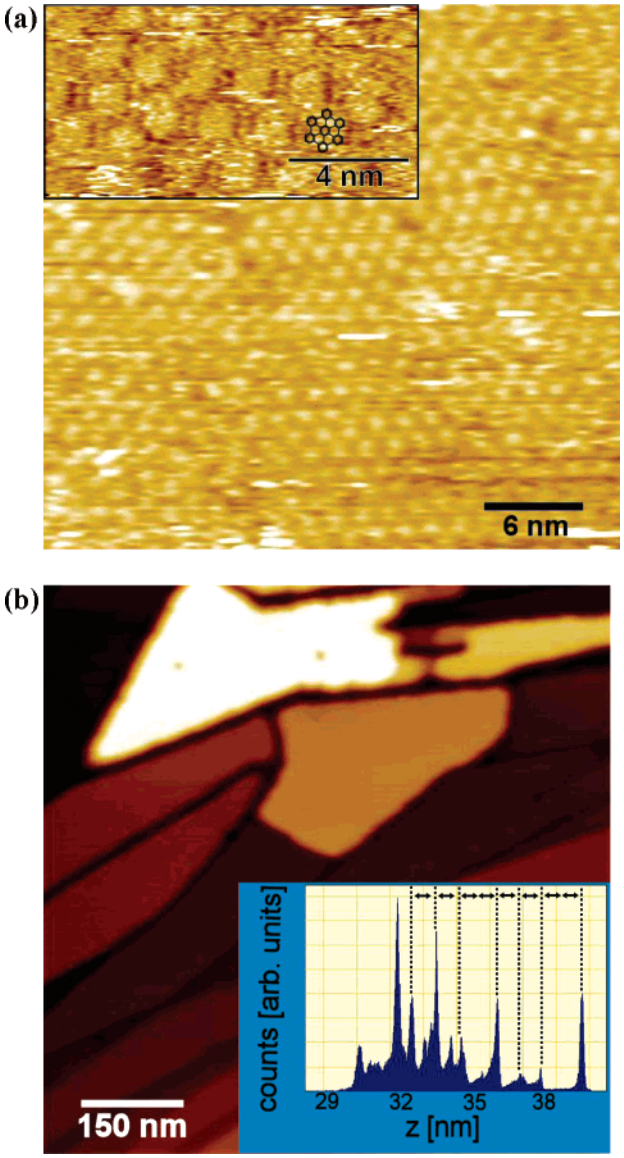

Figure 5. (a) STM image of ca. monolayer HBC on Ag(111) (−1.2 V, 0.4 nA). The short-range order is clearly visible. The inset shows a higher resolution image with one HBC molecule indicated. (b) SFM image (noncontact mode) of multilayer (30 Å) HBC on Ag(111). Step heights derived from the height distribution histogram (inset) are integer multiples of the HBC column width as shown in Figure 4b for model 2.

spectra are thus interpreted as being due to a superposition of these two molecular orientations (see Figure 4b). In order to estimate the ratio of flat lying (proportion A) and inclined (proportion B) HBC molecules in the two samples, we fitted the data of Figure 3 as a superposition with the angles γ_1' and γ_2' fixed

$$I_{\text{total}} = AI_{\pi^*}(\gamma_1' = 0°) + BI_{\pi^*}(\gamma_2' = 43°) \quad (2)$$

As the number of free fitting parameters in eq 2 is identical to that of eq 1, the best fits were identical. For the 6 Å coverage sample, we obtained a ratio of 60% flat lying (A) to 40% inclined (B) molecules, whereas for the 30 Å coverage sample, 43% of the signal was due to lying and 57% due to inclined HBC. Note that the applicability of model 2 requires island-growth (Volmer−Weber type) of HBC on Ag(111), i.e., multilayer formation with inclined molecules setting in before the flat lying monolayer is completed. Consequently, increasing

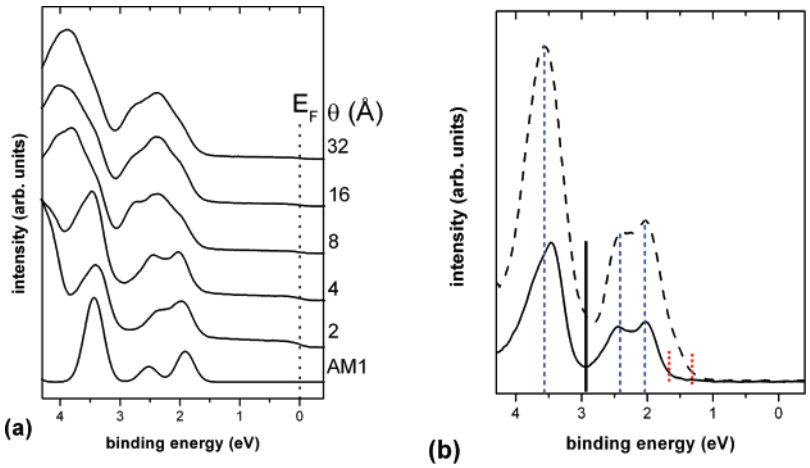

Figure 6. UPS spectra of HBC/Ag(111). (a) Spectra for increasing HBC coverage θ. The bottom spectrum (AM1) is a simulated UPS spectrum of a single molecule. (b) UPS spectra of "clean" monolayer (bottom solid line) and "clean" multilayer (top dashed line) HBC obtained by the subtraction procedure explained in the text. For comparison the multilayer spectrum was shifted by 0.3 eV toward lower binding energy to align the maximum of the highest occupied molecular levels. The two dotted low-BE lines specify the onset of the HOMO-derived photoemission features, and thus indicate the level-broadening due to band formation.

the coverage from 6 Å to 30 Å results in continued growth of the flat lying monolayer and inclined molecules in the multilayer, explaining the still substantial contribution of molecules in the monolayer to the overall spectrum at 30 Å coverage. In fact, this is fully consistent with UPS results presented further below. If layer-by-layer growth were the case, the attenuation of the monolayer component would be stronger than derived above.

Direct support for the validity of model 2 was obtained by STM and SFM investigations. For the monolayer range, STM was used to directly determine the local structure of HBC on Ag(111). At about monolayer coverage (nominal mass thickness 4 Å), HBC spontaneously formed ordered structures on the 10 nm scale, as shown in Figure 5a. However, on larger length scales, a high density of structural defects was observed, which was accompanied by structural instabilities causing changes between subsequently recorded images, which indicates a weak bonding of HBC to the metal surface. Nevertheless, the obtained high-resolution images indicate the packing of individual HBC molecules in a short-range ordered structure with 6-fold symmetry and with lattice constants of $a = b = (1.36 \pm 0.06)$ nm and 2D unit cell angle $\alpha = (60 \pm 2)°$, similar to that observed on other substrates (HOPG,[27] Au(111)[28]). Hence, flat lying molecules in the monolayer could be verified.

For SFM investigations in the multilayer regime, a mass thickness of 30 Å HBC on Ag(111) was chosen. A representative SFM image (Figure 5b) shows islands of large flat terraces with well-defined step edges. In order to derive the height of individual steps present in the image the height-distribution histogram was evaluated (inset of Figure 5b). The step heights were found to be integer multiples of (9 ± 1) Å, which agrees very well the expected height of lying HBC columns consisting of 43° tilted molecules in model 2 (i.e., 8.5 Å as indicated in Figure 4b).

2. Electronic Structure. For UPS, starting with 2 Å HBC nominal coverage (θ) on Ag(111) the mass thickness was doubled after each deposition step up to a final mass thickness of 32 Å (Figure 6a). The valence region spectra for $\theta = 2$ and 4 Å agree well with the simulated spectrum (bottom) of a single HBC molecule in the gas phase, obtained by Gaussian broadening of molecular eigenstates obtained by semiemprirical AM1 calculations,[29] after appropriate adjustment of the energy scale. The photoemission feature at lowest binding energy (BE), centered at 2 eV, is derived from the two degenerate highest occupied π levels of HBC, and the feature at 2.5 eV corresponds to the next deeper lying π level. With increasing θ, an additional peak appears at yet higher binding energy (2.8 eV), whereas the intensity of the peak closest to the Fermi level (E_F) decreases, and the spectrum broadens overall.

A close look at the intensity of the Ag Fermi edge reveals that it is still nonzero at 32 Å HBC mass thickness, indicating an incomplete coverage of the Ag surface with molecules.[30,31] Consequently, island growth for HBC/Ag(111) as postulated in model 2 above is confirmed. The transition from a valence spectral shape resembling single HBC molecules to a more complex shape occurs between 4 and 8 Å mass thickness. Fully consistent with growth model 2, in addition to flat lying HBC in the monolayer, vertically inclined HBC molecules are present for $\theta > 4$ Å. HBC molecules in the multilayer thus give rise to the complex shape of UPS spectra for HBC $\theta \geq 8$ Å.

In order to verify that the photoemission spectra for high coverage are indeed a superposition of mono- and multilayer intrinsic HBC spectra, the following procedure was applied. First, all spectra were normalized to the intensity at the Fermi edge. Subsequently, the scaled pristine Ag(111) spectrum was subtracted from the 4 Å HBC/Ag(111) spectrum in order to derive the photoemission signal from the organic monolayer alone (displayed as bottom curve in Figure 6b). In order to remove metal substrate and HBC monolayer contributions from the 32 Å HBC/Ag(111) spectrum, the scaled 4 Å HBC/Ag(111) spectrum was subtracted. For better comparison, this multilayer spectrum was shifted by 0.3 eV in order to align the lowest BE features (top curve in Figure 6b). The comparison of "clean" HBC mono- (solid line) and multilayer (dashed line) spectra in Figure 6b evidence that the multilayer spectrum is very similar to the monolayer spectrum, except for the 0.3 eV BE shift. The origin of this energy shift of the multilayer compared to the monolayer can be explained by changes of the polarization energy, i.e., weaker photohole screening due to a larger distance from the metal surface.[32] In addition, the "clean" multilayer spectrum exhibits significant broadening of the feature derived from the HBC highest occupied levels toward lower BE (Figure 6b). This may be due to the superposition of several effective multilayer thicknesses (with different screening efficiencies), which cannot be taken into account with our subtraction procedure. Also, the observed broadening of ca. 0.35

eV (Figure 6b) may arise from 1-dimensional electron band formation in the multilayer along the columnar stacking axis due to substantial intermolecular coupling[33] of neighboring HBC molecules in the bulk crystal structure.[7] The clear-cut structural transition from flat lying (monolayer) to vertically inclined (multilayer) orientation of HBC on Ag(111) as proposed in model 2 (Figure 4b) is thus fully supported by UPS results.

Conclusion

The structural and electronic properties at the interface formed between hexa-*peri*-hexabenzocoronene and Ag(111) was investigated by NEXAFS, STM, SFM, and UPS. The following consistent picture of the interface was derived: The monolayer of HBC adsorbs flat lying on the metal surface and the molecular electronic structure resembles that of individual molecules due to weak molecule/metal interaction. Multilayer HBC grows in its bulk crystal structure on the monolayer HBC/Ag(111) template with an angle of 43° between the molecular planes and the substrate surface. This defined mono- to multilayer structural transition is accompanied by a 0.3 eV shift of the molecular levels toward higher binding energy. The formation of dispersing intermolecular electron bands in the crystalline multilayer is indicated by a broadening of the highest occupied HBC levels by ca. 0.35 eV compared to the monolayer, where no significant $\pi-\pi$ intermolecular overlap occurs.

Acknowledgment. This work was in part supported by the European Commission under Contract No. NMP-3-CT-2006-033197 ("ICONTROL") and by the DFG through Sfb 658 "Elementary processes in molecular switches at surfaces". N.K. acknowledges financial support by the Emmy Noether-Program (DFG).

References and Notes

(1) (a) Forrest, S. R. *Nature* **2004**, *428*, 911. (b) Muccini, M. *Nat. Mater.* **2006**, *5*, 605. (c) Koch, N. *ChemPhysChem* **2007**, DOI: 10.1002/cphc.200700177.

(2) Keil, M.; Samori, P.; Santos, D.; Kugler, T.; Stafström, S.; Brand, J.; Müllen, K.; Brédas, J.; Rabe, J. P.; Salaneck, W. *J. Phys. Chem. B* **2000**, *104*, 3967.

(3) Gross, L.; Moresco, F.; Ruffieux, P.; Gourdon, A.; Joachim, C.; Rieder, K. *Phys. Rev. B* **2005**, *71*, 165428.

(4) Ruffieux, P.; Gröning, O.; Bielmann, M.; Simpson, C.; Müllen, K.; Schlapbach, L.; Gröning, P. *Phys. Rev. B* **2002**, *66*, 073409.

(5) Goddard, R.; Haenel, M.; Herndon, W.; Krueger, C.; Zander, M. *J. Am. Chem. Soc.* **1995**, *117*, 30.

(6) Kübel, C.; Eckhardt, K.; Enkelmann, V.; Wegner, G.; Müllen, K. *J. Mater. Chem.* **2000**, *10*, 879.

(7) Friedlein, R.; Crispin, X.; Simpson, C.; Watson, M.; Jäckel, F.; Osikowicz, W.; Marciniak, S.; Jong, M.; Samori, P.; Jönsson, S.; Fahlman, M.; Müllen, K.; Rabe, J. P.; Salaneck, W. R. *Phys. Rev. B* **2003**, *68*, 195414.

(8) Lemaur, V.; Da, Silva, Filho, D. A.; Coropceanu, V.; Lehmann, M.; Geerts, Y.; Piris, J.; Debije, M. G.; Van, de Craats, A. M.; Senthilkumar, K.; Siebbeles, L. D. A.; Warman, J. M.; Bredas, J. L.; Cornil, J. *J. Am. Chem. Soc.* **2004**, *126*, 3271.

(9) Van, de Craats, A. M.; Warman, J. M.; Fechtenkötter, A.; Brand, J. D.; Harbison, M. A.; Müllen, K. *Adv. Mater.* **2004**, *11*, 1469.

(10) Ito, S.; Wehmeier, M.; Brand, J.; Kübel, C.; Epsch, R.; Rabe, J.; Müllen, K. *Chem. Eur. J.* **2000**, *6*, 4327.

(11) Fleming, A.; Coleman, J.; Dalton, A.; Fechtenkötter, A.; Watson, M.; Müllen, K.; Byrne, H.; Blau, W. *J. Phys. Chem. B* **2003**, *107*, 37.

(12) Jäckel, F.; Watson, M. D.; Müllen, K.; Rabe, J. P. *Phys. Rev. B* **2006**, *73*, 045423.

(13) Stabel, A.; Herwig, P.; Müllen, K.; Rabe, J. P. *Angew. Chem., Int. Ed. Engl.* **1995**, *34* 1609; *Angew. Chem.* **1995**, *107*, 1768.

(14) Jäckel, F.; Wang, Z.; Watson, M. D.; Müllen, K.; Rabe, J. P. *Chem. Phys. Lett.* **2004**, *387*, 372.

(15) Jäckel, F.; Watson, M. D.; Müllen, K.; Rabe, J. P. *Phys. Rev. Lett.* **2004**, *92*, 188303.

(16) Schöll, A.; Zou, Y.; Schmidt, T.; Fink, R.; Umbach, E. *J. El. Spec.* **2003**, *129*, 1.

(17) Luo, Y.; Ågren, H.; Keil, M.; Friedlein, R.; Salaneck, W. *Chem. Phys. Lett.* **2001**, *337*, 176.

(18) Stöhr, J. *NEXAFS Spectroscopy*; Springer: New York, 2003.

(19) Yannoulis, P.; Dudde, R.; Frank, K.; Koch, E. E. *Surf. Sci.* **1987**, *189/190*, 519.

(20) Kiel, M.; Duncker, K.; Hagendorf, C.; Widdra, W. *Phys. Rev. B* **2007**, *75*, 195439.

(21) Duhm, S.; Glowatzki, H.; Johnson, R. L.; Rabe, J. P.; Koch, N. *Appl. Phys. Lett.* **2006**, *88*, 203109.

(22) McDonald, O.; Cafolla, A.; Carty, D.; Sheerin, G.; Hughes, G. *Surf. Sci.* **2006**, *600*, 3217.

(23) Witte, G.; Wöll, Ch. *J. Mater. Res.* **2004**, *19*, 1889.

(24) Proehl, H.; Toerker, M.; Sellam, F.; Fritz, T.; Leo, K.; Simpson, C.; Müllen, K. *Phys. Rev. B* **2001**, *63*, 205409.

(25) Beernink, G.; Strunskus, T.; Witte, G.; Wöll, Ch. *Appl. Phys. Lett.* **2004**, *85*, 398.

(26) Koch, N.; Salzmann, I.; Johnson, R. L.; Pflaum, J.; Friedlein, R.; Rabe, J. P. *Organ. Elec.* **2006**, *7*, 537.

(27) Samori, P.; Severin, N.; Simpson, C.; Müllen, K.; Rabe, J. *J. Am. Chem. Soc.* **2002**, *124*, 9454.

(28) Sellam, F.; Schmitz-Hübsch, T.; Toerkera, M.; Mannsfeld, S.; Proehl, H.; Fritz, T.; Leo, K.; Simpson, C.; Müllen, K. *Surf. Sci.* **2001**, *478*, 113.

(29) Frisch, M. J.; et al. *Gaussian 98*; Gaussian Inc.: Pittsburgh, PA, 2001.

(30) Witte, G.; Hänel, K.; Söhnchen, S.; Wöll, Ch. *Appl. Phys. A* **2006**, *82*, 447.

(31) Krause, B.; Dürr, A. C.; Ritley, K.; Schreiber, F.; Dosch, H.; Smilgies, D. *Phys. Rev. B* **2002**, *66*, 235404.

(32) Koch, N.; Heimel, G.; Wu, J.; Zojer, E.; Johnson, R. L.; Brédas, J. L.; Müllen, K.; Rabe, J. P. *Chem. Phys. Lett.* **2005**, *413*, 390.

(33) Koch, N.; Vollmer, A.; Salzmann, I.; Rabe, J. P.; Weiss, H.; Nickel, B. *Phys. Rev. Lett.* **2006**, *96*, 156803.